

The effect of Carrier Doping and Thickness on the Electronic Structures of $\text{La}_3\text{Ni}_2\text{O}_7$ Thin Films

Haoliang Shi^{1,‡}, Zihao Huo^{1,‡}, Guanlin Li¹, Hao Ma¹, Tian Cui^{1,2,*}, Dao-Xin Yao^{3,*}, Defang Duan^{1,*}

¹*Key Laboratory of Material Simulation Methods & Software of Ministry of Education, State Key Laboratory of Superhard Materials, College of Physics, Jilin University, Changchun 130012, China*

²*Institute of High Pressure Physics, School of Physical Science and Technology, Ningbo University, Ningbo 315211, China*

³*Center for Neutron Science and Technology, Guangdong Provincial Key Laboratory of Magnetoelectric Physics and Devices, State Key Laboratory of Optoelectronic Materials and Technologies, School of Physics, Sun Yat-Sen University, Guangzhou, 510275, China*

[‡]These authors contributed equally: Haoliang Shi, Zihao Huo

*Corresponding authors: cuitian@nbu.edu.cn (T. C.), yaodaox@mail.sysu.edu.cn (D. X. Y.), duandf@jlu.edu.cn (D. D.)

Abstract: Recently, the superconductivity of bilayer nickelate $\text{La}_3\text{Ni}_2\text{O}_7$ has been observed in the thin film at ambient pressure, facilitated by epitaxial strain. Here, we investigate the effects of film thickness and carrier doping on the electronic structure of $\text{La}_3\text{Ni}_2\text{O}_7$ thin films with thickness of 0.5-3 unit cells (UC) using first-principles calculations. At an optimal doping concentration of 0.4 holes per formula unit for 2UC film, the Ni- d_{z^2} interlayer bonding state metallizes, leading to the formation of γ pockets at the Fermi surface, which quantitatively matches the experimental results of angle-resolved photoemission spectroscopy (ARPES). These findings provide theoretical support for recent experimental observations of ambient-pressure superconductivity in $\text{La}_3\text{Ni}_2\text{O}_7$ thin films and highlight the crucial role of film thickness and carrier doping in modulating electronic properties.

Keywords: nickelate superconductors, density functional theory, thin films, carrier doping

1 Introduction

Bilayer Ruddlesden-Popper (RP) phase $\text{La}_3\text{Ni}_2\text{O}_7$ has been observed with a T_c of about 80 K at high pressure [1-5], becoming the second unconventional superconductor family with T_c higher than the boiling temperature of liquid nitrogen. Further structural analysis suggested that $\text{La}_3\text{Ni}_2\text{O}_7$ undergoes a structural transition from the ambient-pressure $Amam$ phase to the high-pressure $Fmmm$ or $I4/mmm$ phase [6,7]. The related superconducting mechanism has been widely discussed [8-30]. Density functional theory (DFT)+U calculations show that additional Ni- d_{z^2} orbitals emerge near the Fermi level (E_F) that are vital for the high T_c , and suggested that the metallization of Ni- d_{z^2} orbitals is important to the superconductivity [1,31]. It also corresponds to a pressure-driven Lifshitz transition. The Hall resistivity measurement of $\text{La}_3\text{Ni}_2\text{O}_7$ at high pressures provides evidence for the Ni- d_{z^2} electronic dynamics in the formation of superconductivity [3].

Although $\text{La}_3\text{Ni}_2\text{O}_7$ exhibits a high temperature superconductivity, its superconducting phase can only be observed under high pressures. This high-pressure condition poses significant challenges to investigate the underlying superconductivity mechanism. Introducing strain into $\text{La}_3\text{Ni}_2\text{O}_7$ has been suggested as an effective way to obtain superconductivity at ambient pressure. For example, DFT calculation suggested that introducing compressive strain along c axis [31] or tensile strain along a and b axis [32] would benefit for the superconductivity in bulk $\text{La}_3\text{Ni}_2\text{O}_7$. Recently, $\text{La}_3\text{Ni}_2\text{O}_7$, $\text{La}_{2.85}\text{Pr}_{0.15}\text{Ni}_2\text{O}_7$, and $\text{La}_2\text{PrNi}_2\text{O}_7$ thin films, with the help from the epitaxial strain imposed on the LaSrAlO (LSAO) substrates, show superconductivity above the MacMillan limit (≈ 40 K) at atmospheric pressure[33].

In these thin film systems, precision ozone annealing is important for the emergence of the superconductivity, which can adjust the ozone content and provide holes. Additionally, Sr substitution of La near the interface due to interfacial diffusion from the LSAO substrate may introduce moderate hole doping into the system. Besides, experimentalists observed the thickness of one to three unit cells (UC), exhibiting tetragonal symmetry [34], but orthogonal symmetry could not be ruled out [33]. The ARPES experiments reveal that the γ pockets (Ni- d_{z^2} orbital) in the $\text{La}_{2.85}\text{Pr}_{0.15}\text{Ni}_2\text{O}_7$

films are metallized [35]. Given that the metallicity of the Ni- d_{z^2} orbital at the Fermi surface plays a pivotal role in achieving superconductivity in bilayer nickelate systems, both film thickness and carrier doping can cause significant changes in the electronic structure of the thin film nickelate. Consequently, it is crucial to systematically evaluate how the electronic structure of the ideal bilayer Ruddlesden-Popper phase nickelate evolves with doping concentrations and film thicknesses.

In this study, we investigate the electronic structure of bilayer RP phase nickelates with thicknesses ranging from simple model of 0.5 to 3UC using the DFT+U method. The results show that the Ni- d_{z^2} interlayer bonding state becomes metallic for 1-3UC with 0.4 holes per formula unit (f.u.). Additionally, the Fermi surface adopts a topological morphology resembling that of the bulk under high-pressure, indicative of potential superconductivity. We propose that hole doping is important for modulating the electronic structure and enabling favorable conditions for novel electronic phases. Our findings provide valuable insights for future experiments, highlighting that appropriate hole doping can facilitate the induction of superconductivity in bilayer RP-phase nickelate thin films.

2 Computational details

We perform first-principles calculations based on a density-functional theory as implemented in VASP code [36]. We adopt the PBE exchange-correlation generalization under the generalized gradient approximation and the PAW pseudopotentials with La, Ni, and O corresponding to valence electrons $5s^25p^65d^16s^2$, $3s^23p^63d^84s^2$, and $2s^22p^2$ [37,38]. In order to consider the in-situ Coulomb repulsion effect of Ni atoms, we applied the $U=3.5$ eV on Ni atoms to simulate the static correlation effect [39,40]. To balance the efficiency and accuracy, we use a cutoff energy of 700 eV and a $2\pi \times 0.03 \text{ \AA}^{-1}$ sampling grid of K-points in the Brillouin zone to ensure energy convergence. We build the crystal structure of the 0.5-3UC films of $\text{La}_3\text{Ni}_2\text{O}_7$ according to the experimentally measured structural parameters using crystal structure slices of tetragonal (I4/mmm) phase and orthorhombic (Amam) phase. For tetragonal phase, we use $a=b=3.77 \text{ \AA}$, while for orthorhombic phase, we use $a=5.36 \text{ \AA}$

and $b= 5.30 \text{ \AA}$. In the direction perpendicular to the bilayer, we use a vacuum layer of 20 \AA . We fix the lattice constants in the a and b directions and optimize the atomic positions. To account for carrier doping effects due to interface effects, substrate Sr diffusion, etc., we simulate doping effects using 0.2 electron to 1 hole per chemical formula.

3 Results and discussion

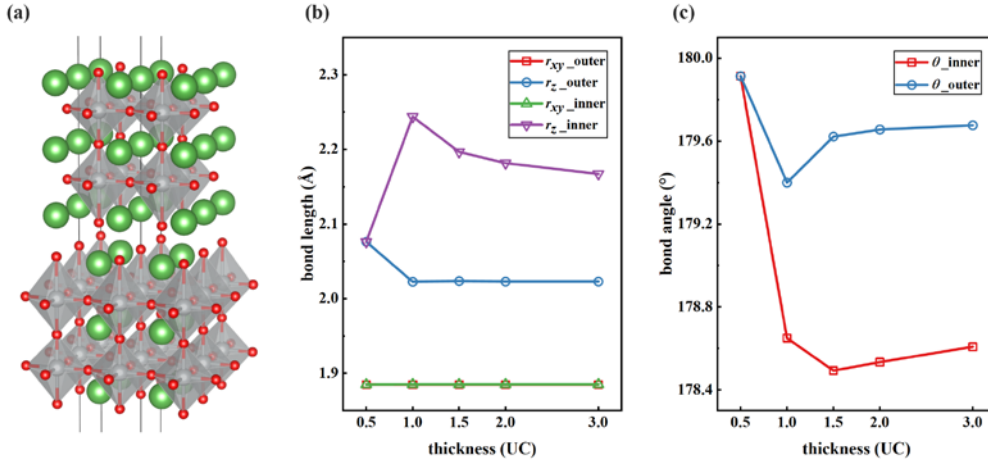


FIG 1 The structure and geometry properties of tetragonal $\text{La}_3\text{Ni}_2\text{O}_7$ thin film. (a) The structure of 1UC $\text{La}_3\text{Ni}_2\text{O}_7$ thin film. The green, silver, and red spheres represent La, Ni, and O atoms, respectively. (b) The Ni-O bond lengths as a function of the film thickness. Red square, blue circle, green upward triangle, and purple downward triangle represent r_{xy} of the surface layer, r_z of the surface layer, r_{xy} of the inner layer, and r_z of the inner layer, respectively, (c) The red square and blue circle represent the Ni-O-Ni bond angles of the outer and inner layers as a function of the film thickness, respectively.

We choose the experimentally measured lattice constants and construct the structure model of thin film with thickness of 0.5-3UC. Figure 1a shows the tetragonal structured thin film with thickness of 1UC as an example. Fig. 1b represents the in-plane Ni-O bond lengths (r_{xy}) and out-of-plane Ni-O bond length (r_z) in inner and outer layers as a function of the film thickness. We found that the r_{xy} of inner and outer layers are similar in all thickness we studied. When the thickness is larger than 0.5UC, the r_z of the inner layer is always longer than that of the outer layer, and the difference between them gradually decreases as the thickness increases. The difference between these two layers decreases from 0.22 to 0.144 \AA when the thickness increases from 1 to 3UC. Figure 1c shows the in-plane Ni-O-Ni bond angles (θ) as a function of the film

thickness. We can find that the θ of the outer layers is larger than that of the inner layers in the thickness of 1-3UC. Therefore, the difference of the r_z and θ suggested that the surface reconstruction exists in the outermost layer of the $\text{La}_3\text{Ni}_2\text{O}_7$ thin films, which may result in different properties compared with bulk compound at high pressure.

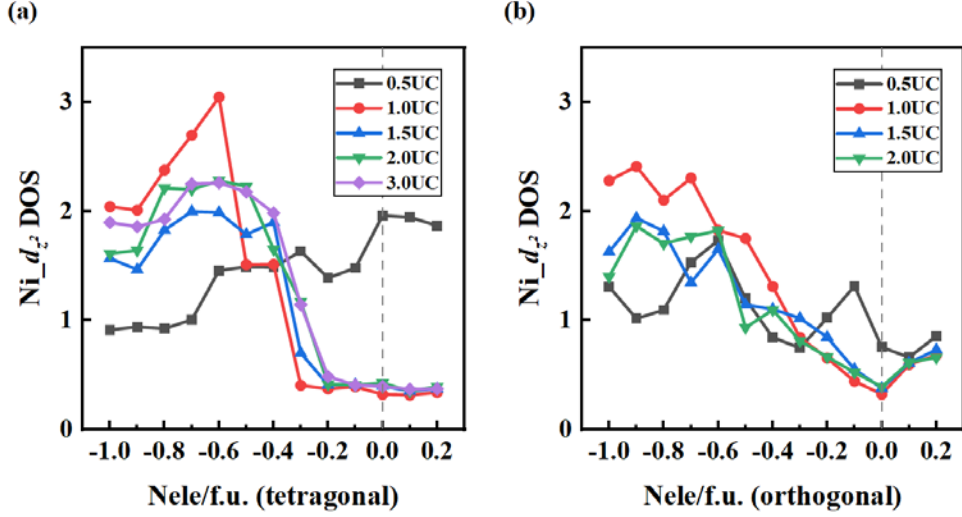


FIG 2 The density of states of $\text{Ni-}d_{z^2}$ at the Fermi level as a function of carrier doping concentration of (a) tetragonal and (b) orthogonal symmetry. Black square, red circle, blue upward triangle, green downward triangle, and purple diamond represent 0.5UC, 1.0UC, 1.5UC, 2.0UC, and 3.0UC film thickness, respectively.

We then calculated the $\text{Ni-}d_{z^2}$ DOS at Fermi level with different film thickness as a function of the carrier doping concentration, as shown in Fig. 2. The carrier doping concentration is ranged from 0.2 electrons to 1.0 holes per formula unit, corresponding to a nominal Ni valence state from 2.6 to 2.0. For the tetragonal phase, when the film thickness is 0.5UC, the $\text{Ni-}d_{z^2}$ DOS reaches its maximum value for the undoped case, while for both electron and hole dopings, it decreases with increasing doping concentration. It means that doping current carriers into 0.5UC model would reduce the $\text{Ni-}d_{z^2}$ DOS at Fermi level and may not be conducive to superconductivity. For the film thickness of 1UC, when the electron doping concentration increases from 0 to 0.2 ele/f.u., the $\text{Ni-}d_{z^2}$ DOS slightly increases. Therefore, electron doping has almost no effect to the $\text{Ni-}d_{z^2}$ DOS. For the hole doping, the $\text{Ni-}d_{z^2}$ DOS at Fermi level remains almost constant as the doping concentration increases. When the doping concentration reaches 0.4 hole/f.u. (0.2 hole/Ni), the DOS value suddenly increases to 1.5 states eV^{-1} f.u. $^{-1}$. As the hole doping concentration further increases, the $\text{Ni-}d_{z^2}$ DOS increases,

reaching its maximum value of 3.05 states $\text{eV}^{-1} \text{f.u.}^{-1}$ at 0.6 hole/f.u., and then it decreases. For the film thickness of 1.5-3UC, the relationship between the Ni- d_{z^2} DOS and the doping concentration is similar to that of 1UC thickness, and the maximum value of their Ni- d_{z^2} DOS happens at 0.6 hole/f.u. (1.99 states $\text{eV}^{-1} \text{f.u.}^{-1}$ for 1.5UC, 2.28 states $\text{eV}^{-1} \text{f.u.}^{-1}$ for 2UC, 2.26 states $\text{eV}^{-1} \text{f.u.}^{-1}$ for 3UC).

For orthogonal phase, when the film thickness is 0.5UC, the Ni- d_{z^2} DOS has a value of 0.75 states $\text{eV}^{-1} \text{f.u.}^{-1}$ for the undoped case. Doping with 0.2 ele/f.u. or 0.6 hole/f.u. will cause the Ni- d_{z^2} DOS to peak at 0.85 and 1.73 states $\text{eV}^{-1} \text{f.u.}^{-1}$, respectively. For the 1UC film, when the doping concentration of electrons increases from 0 to 0.2 ele/f.u., the Ni- d_{z^2} DOS increases from 0.32 states $\text{eV}^{-1} \text{f.u.}^{-1}$ to 0.68 states $\text{eV}^{-1} \text{f.u.}^{-1}$. Therefore, electron doping has less effect on the Ni- d_{z^2} DOS. As the hole doping concentration increases, the Ni- d_{z^2} DOS increases, reaching its maximum value of 2.41 states $\text{eV}^{-1} \text{f.u.}^{-1}$ at 0.9 hole/f.u., and then it gets decreased. For the 1.5-3UC films, the relationship between the Ni- d_{z^2} DOS and the doping concentration is similar with that of 1UC film, and the maximum value of their Ni- d_{z^2} DOS reaches at 0.9 hole/f.u. (1.943 states $\text{eV}^{-1} \text{f.u.}^{-1}$ for 1.5UC model, 1.86 states $\text{eV}^{-1} \text{f.u.}^{-1}$ for 2UC model).

These results indicate that when the film thickness exceeds 1UC, the geometric parameters and DOS do not vary significantly with the thickness. Moreover, hole doping with proper concentration helps to increase the Ni- d_{z^2} DOS of thin film with thickness of 1-3UC, thus making it a potential superconductor. Therefore, we will focus on the electronic structure of 1-3UC in the following text.

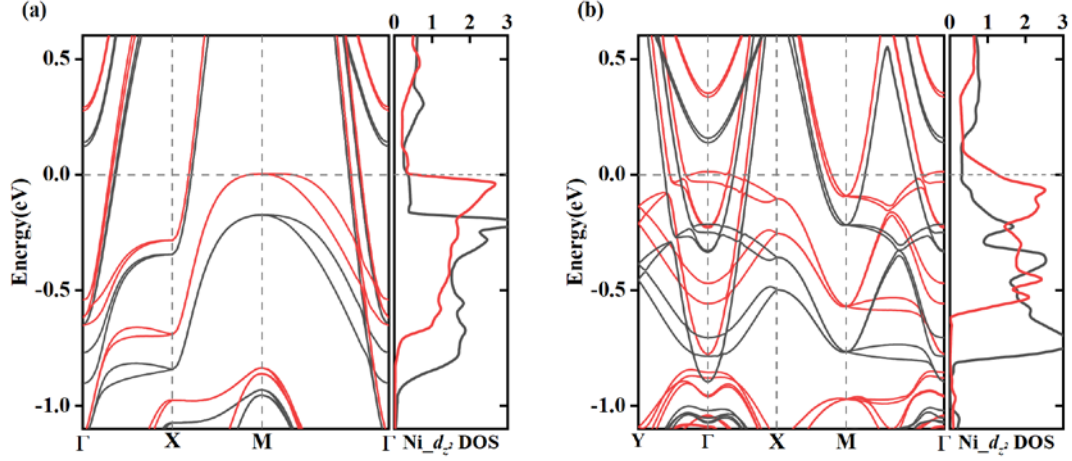


FIG 3 Electronic properties of the tetragonal (left) and orthogonal (right) phases without (black solid line) and with 0.4 hole/f.u. doping (red solid line) for the 1UC film.

Figure 3 shows the electronic structures and Ni- d_{z^2} DOS of tetragonal and orthogonal phases without and with 0.4 hole/f.u. doping. In both tetragonal and orthogonal phases, the energy of Ni- $d_{x^2-y^2}$ and Ni- d_{z^2} bands increase, which is different from the self-doping effect that exists in the bulk $\text{La}_3\text{Ni}_2\text{O}_7$ under high pressure [1]. Besides, the Ni- d_{z^2} interlayer bonding state cross the Fermi level and a small hole Fermi pocket emerge around the M point for tetragonal phase and Γ point for orthogonal phase, which is crucial for the emergence of superconductivity in bulk compound at high pressure[13,20,25,41]. The Ni- d_{z^2} DOS at Fermi level is 1.51 (1.31) states $\text{eV}^{-1} \text{f.u.}^{-1}$ for tetragonal (orthogonal) phase, which is comparable to that of the bulk $I4/mmm$ phase at 30 GPa (2.2 states $\text{eV}^{-1} \text{f.u.}^{-1}$)[31]. The high DOS at E_F and the existence of the hole Fermi pocket make the thin film with doping concentration of 0.4 hole/f.u. a candidate superconductor.

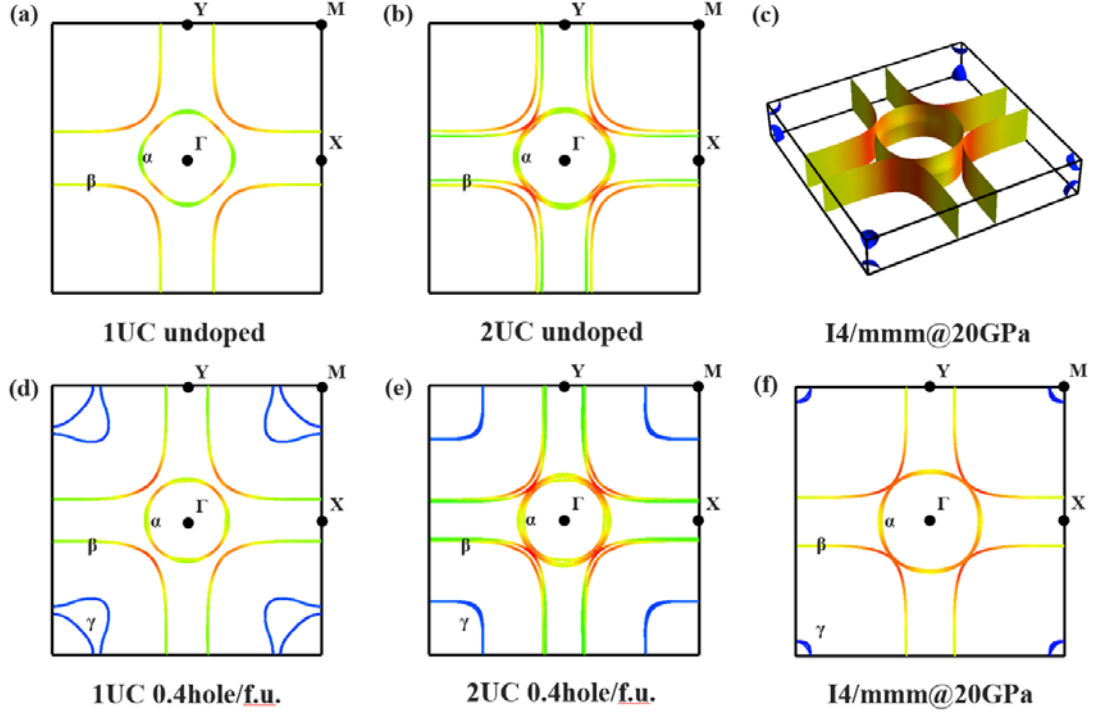


FIG 4 Fermi surface of the tetragonal phase with different thickness and doping concentration. The colors projected onto the Fermi surface represent the Fermi velocity. (a) 1UC without doping, (b) 2UC without doping, (c) tetragonal phase at 20 GPa, (d) 1UC with 0.4 hole/f.u., (e) 2UC with 0.4 hole/f.u., (f) The Fermi surface slice in the (0 0 0.5) plane for the bulk tetragonal phase under 20 GPa.

According to the previous studies, the Fermi surface of bulk $\text{La}_3\text{Ni}_2\text{O}_7$ under high pressure can have three fermi sheets[13]: the α and β pockets dominated by the $\text{Ni-}d_{x^2-y^2}$ orbitals, and the γ -pocket dominated by the $\text{Ni-}d_{z^2}$ orbital, which emerges near the M-points proposed to play a critical role in superconductivity. In the thin-film system, symmetry breaking leads to changes in the Fermi surface topology. For 1UC-thick films, the α and β pockets undergo a degeneracy lifting along the Γ -M path, indicating a disruption of the symmetry compared to the bulk material. However, for thicker films (greater than 1UC), the α and β pockets shift closer to each other along the Γ -M path, resulting in a Fermi surface that becomes more degenerate and similar with that of bulk compound at high pressure. For hole-doped systems (Fig. 4d, e), doping 0.4 hole/f.u. could causes a Lifshitz transition hole-Fermi-pocket formation at the Fermi surface around the M point, corresponding to the metallization of the $\text{Ni-}d_{z^2}$ energy band. And the γ pocket becomes significantly larger compared to that of bulk

structure at 20 GPa. The degeneracy of the γ pocket varies with film thickness. For 1UC thick films, the γ pocket splits, similar to the splitting of the α and β pockets in the undoped case. In contrast, for thicker films (2-3UC), the degeneracy of γ pocket increases, approaching the symmetry observed in the bulk material. Notably, the Fermi surface of the 2UC film doped with 0.4 hole/f.u. (0.2 hole/Ni) (Fig 4e) is in good agreement with the ARPES measurements [35], sharing comparable size and topological features. And the hole doping of 0.2 hole/Ni is also consistent with the experimental results. The interplay between film thickness and doping concentration thus becomes a key factor in tuning electronic properties of $\text{La}_3\text{Ni}_2\text{O}_7$ thin films, which could be crucial for potential experimental studies aiming to optimize its electronic characteristics for novel applications.

4 Conclusions

In summary, we have performed a comprehensive first-principles study on the effects of film thickness and carrier doping on the electronic structure of $\text{La}_3\text{Ni}_2\text{O}_7$ thin films with thickness of 0.5-3UC. Our results show that the 1-3UC films with optimal doping levels lead to the metallization of the $\text{Ni-}d_{z^2}$ and the formation of γ pockets at the Fermi surface. The 2UC film doped with 0.4 hole/f.u. quantitatively match the Fermi surfaces from ARPES experiments. Our work provides a theoretical framework that aligns with recent experimental observations of ambient-pressure superconductivity in $\text{La}_3\text{Ni}_2\text{O}_7$ thin films. It emphasizes the importance of carrier doping, paving the way for future experimental and theoretical investigations.

Acknowledgments

We thank Zhuoyu Chen and Yuefeng Nie for the experimental data and discussion and thank Weiqiang Chen for many stimulating discussions. This work was supported by National Key R&D Program of China (Nos. 2022YFA1402304 and 2022YFA1402802), National Natural Science Foundation of China (Grants Nos. 12494591, 12122405, 12274169, and 92165204), Program for Science and Technology Innovation Team in Zhejiang (Grant No. 2021R01004), Guangdong Provincial Key

Laboratory of Magnetoelectric Physics and Devices (Grant No. 2022B1212010008), Research Center for Magnetoelectric Physics of Guangdong Province (2024B0303390001), Guangdong Provincial Quantum Science Strategic Initiative (GDZX2401010), and the Fundamental Research Funds for the Central Universities. Some of the calculations were performed at the High Performance Computing Center of Jilin University and using TianHe-1(A) at the National Supercomputer Center in Tianjin.

Note added. After completing this work, we became aware of three independent studies on superconductivity in $\text{La}_3\text{Ni}_2\text{O}_7$ thin films. Those studies focus on different models and property of the thin films. Shao et al. investigated the pairing symmetry of the bulk *Amam* model, excluding the γ hole pocket around the M point, using a either-band tight-binding model[42]. Yue et al. developed a realistic multi-orbital Hubbard model for 0.5UC films and employed density functional theory (DFT) combined with cluster dynamical mean-field theory (CDMFT) to calculate the pairing symmetry and mechanism[43]. Le et al. explored superconductivity and charge density wave states in 3UC $\text{La}_3\text{Ni}_2\text{O}_7$ films on SLAO substrates[44]. Our work systematically examines both carrier doping and film thickness in $\text{La}_3\text{Ni}_2\text{O}_7$ thin films, emphasizing the critical role of doping effects and optimal thickness in electronic properties.

References

- [1] H. Sun, M. Huo, X. Hu, J. Li, Z. Liu, Y. Han, L. Tang, Z. Mao, P. Yang, B. Wang, J. Cheng, D.-X. Yao, G.-M. Zhang and M. Wang, *Nature* 621 (7979), 493-498 (2023).
- [2] J. Hou, P. Yang, Z. Liu, J. Li, P. Shan, L. Ma, G. Wang, N. Wang, H. Guo, J. Sun, Y. Uwatoko, M. Wang, G. Zhang, B. Wang and J. Cheng, *Chin. Phys. Lett.* 40 (11), 117302 (2023).
- [3] Y. Zhang, D. Su, Y. Huang, Z. Shan, H. Sun, M. Huo, K. Ye, J. Zhang, Z. Yang, Y. Xu, Y. Su, R. Li, M. Smidman, M. Wang, L. Jiao and H. Yuan, *Nature Physics* (2024).
- [4] Y. Zhou, J. Guo, S. Cai, H. Sun, P. Wang, J. Zhao, J. Han, X. Chen, Q. Wu, Y. Ding, M. Wang, T. Xiang, H. Mao and L. Sun, *Arxiv preprint arXiv:2311.12361* (2023).
- [5] G. Wang, N. N. Wang, X. L. Shen, J. Hou, L. Ma, L. F. Shi, Z. A. Ren, Y. D. Gu, H. M. Ma, P. T. Yang, Z. Y. Liu, H. Z. Guo, J. P. Sun, G. M. Zhang, S. Calder, J. Q. Yan, B. S. Wang, Y. Uwatoko and J. G. Cheng, *Physical Review X* 14 (1), 011040 (2024).
- [6] L. Wang, Y. Li, S.-Y. Xie, F. Liu, H. Sun, C. Huang, Y. Gao, T. Nakagawa, B. Fu, B. Dong, Z. Cao, R. Yu, S. I. Kawaguchi, H. Kadobayashi, M. Wang, C. Jin, H.-k. Mao and H. Liu, *Journal of the American Chemical Society* 146 (11), 7506-7514 (2024).
- [7] J. Li, P. Ma, H. Zhang, X. Huang, C. Huang, M. Huo, D. Hu, Z. Dong, C. He, J. Liao, X. Chen, T. Xie, H. Sun and M. Wang, *ArXiv preprint arXiv:2404.11369* (2024).
- [8] Z. Luo, X. Hu, M. Wang, W. Wú and D.-X. Yao, *Physical Review Letters* 131 (12), 126001 (2023).
- [9] Y. Gu, C. Le, Z. Yang, X. Wu and J. Hu, *Arxiv preprint arXiv:2306.07275* (2023).
- [10] Q.-G. Yang, D. Wang and Q.-H. Wang, *Physical Review B* 108 (14), L140505 (2023).
- [11] D. A. Shilenko and I. V. Leonov, *Physical Review B* 108 (12), 125105 (2023).
- [12] X. Chen, P. Jiang, J. Li, Z. Zhong and Y. Lu, *ArXiv preprint arXiv:2307.07154* (2023).
- [13] Y.-B. Liu, J.-W. Mei, F. Ye, W.-Q. Chen and F. Yang, *Physical Review Letters* 131 (23), 236002 (2023).
- [14] V. Christiansson, F. Petocchi and P. Werner, *Physical Review Letters* 131 (20), 206501 (2023).
- [15] Y. Zhang, L.-F. Lin, A. Moreo and E. Dagotto, *Physical Review B* 108 (18), L180510 (2023).
- [16] Z. Liao, L. Chen, G. Duan, Y. Wang, C. Liu, R. Yu and Q. Si, *Physical Review B* 108 (21), 214522 (2023).
- [17] F. Lechermann, J. Gondolf, S. Bötzel and I. M. Eremin, *Physical Review B* 108 (20), L201121 (2023).
- [18] Y. Shen, M. Qin and G.-M. Zhang, *Chinese Physics Letters* 40 (12), 127401 (2023).
- [19] Y.-f. Yang, G.-M. Zhang and F.-C. Zhang, *Physical Review B* 108 (20), L201108 (2023).
- [20] J. Huang, Z. D. Wang and T. Zhou, *Physical Review B* 108 (17), 174501 (2023).
- [21] Q. Qin and Y.-f. Yang, *Physical Review B* 108 (14), L140504 (2023).
- [22] Z. Luo, B. Lv, M. Wang, W. Wu and D. Yao, *arXiv preprint arXiv:2308.16564* (2023).

- [23] C. Lu, Z. Pan, F. Yang and C. Wu, *Physical Review Letters* 132 (14), 146002 (2024).
- [24] Y. Zhang, L.-F. Lin, A. Moreo, T. A. Maier and E. Dagotto, *Nature Communications* 15 (1), 2470 (2024).
- [25] W. Wú, Z. Luo, D.-X. Yao and M. Wang, *Science China Physics, Mechanics & Astronomy* 67 (11), 117402 (2024).
- [26] H. Sakakibara, N. Kitamine, M. Ochi and K. Kuroki, *Physical Review Letters* 132 (10), 106002 (2024).
- [27] X.-Z. Qu, D.-W. Qu, J. Chen, C. Wu, F. Yang, W. Li and G. Su, *Physical Review Letters* 132 (3), 036502 (2024).
- [28] K. Jiang, Z. Wang and F.-C. Zhang, *Chinese Physics Letters* 41 (1), 017402 (2024).
- [29] Y. Cao and Y.-f. Yang, *Physical Review B* 109 (8), L081105 (2024).
- [30] Y.-H. Tian, Y. Chen, J.-M. Wang, R.-Q. He and Z.-Y. Lu, *Physical Review B* 109 (16), 165154 (2024).
- [31] Z. H. Huo, Z. H. Luo, P. Zhang, A. Q. Yang, Z. T. Liu, X. R. Tao, Z. H. Zhang, S. M. Guo, Q. W. Jiang, W. X. Chen, D. X. Yao, D. F. Duan and T. Cui, *Science China-Physics Mechanics & Astronomy* 68 (3) (2025).
- [32] B. Geisler, J. J. Hamlin, G. R. Stewart, R. G. Hennig and P. J. Hirschfeld, *arXiv preprint arXiv:2411.14600* (2024).
- [33] E. K. Ko, Y. Yu, Y. Liu, L. Bhatt, J. Li, V. Thampy, C.-T. Kuo, B. Y. Wang, Y. Lee, K. Lee, J.-S. Lee, B. H. Goodge, D. A. Muller and H. Y. Hwang, *Nature* (2024).
- [34] L. Bhatt, A. Y. Jiang, E. K. Ko, N. Schnitzer, G. A. Pan, D. Šegedin, Y. Liu, Y. Yu, Y.-F. Zhao, E. A. Morales, C. M. Brooks, A. S. Botana, H. Y. Hwang, J. A. Mundy, D. A. Muller, and B. H., *arXiv preprint arXiv: 2501.08204* (2025)..
- [35] P. Li, G. Zhou, W. Lv, Y. Li, C. Yue, H. Huang, L. Xu, J. Shen, Y. Miao, W. Song, Z. Nie, Y. Chen, H. Wang, W. Chen, Y. Huang, Z.-H. Chen, T. Qian, J. Lin, J. He, Y. Sun, Z. Chen, and Q.-K. Xue, *arXiv preprint arXiv:2501.09255* (2025).
- [36] G. Kresse and J. Furthmüller, *Computational Materials Science* **6**, 15 (1996).
- [37] P. E. Blöchl, *Physical Review B* **50**, 17953 (1994).
- [38] J. P. Perdew, K. Burke, and M. Ernzerhof, *Physical Review Letters* **77**, 3865 (1996).
- [39] S. L. Dudarev, G. A. Botton, S. Y. Savrasov, C. J. Humphreys, and A. P. Sutton, *Physical Review B* **57**, 1505 (1998).
- [40] A. I. Liechtenstein, V. I. Anisimov, and J. Zaanen, *Physical Review B* **52**, R5467 (1995).
- [41] H. Oh and Y.-H. Zhang, *Physical Review B* **108**, 174511 (2023).
- [42] Z.-Y. Shao, Y.-B. Liu, M. Liu, and F. Yang, *arXiv preprint arXiv:2501.10409v1* (2025).
- [43] C. Yue, J.-J. Miao, H. Huang, Y. Hua, P. Li, Y. Li, G. Zhou, W. Lv, Q. Yang, H. Sun, Y. Sun, J. Lin, Q.-K. Xue, Z. Chen, and W. Chen, *arXiv preprint arXiv:2501.06875v1* (2025).
- [44] C. Le, J. Zhan, X. Wu, and J. Hu, *arXiv preprint arXiv:2501.14665v1* (2025).